



HAL
open science

Redox-switching of ternary Ni(ii) and Cu(ii) complexes synthesis, experimental and theoretical studies along with second-order nonlinear optical properties

Néstor Novoa, Carolina Manzur, Thierry Roisnel, Vincent Dorcet, Nolwenn Cabon, Françoise Robin-Le Guen, Isabelle Ledoux-Rak, Samia Kahlal, Jean-Yves Saillard, David Carrillo, et al.

► To cite this version:

Néstor Novoa, Carolina Manzur, Thierry Roisnel, Vincent Dorcet, Nolwenn Cabon, et al.. Redox-switching of ternary Ni(ii) and Cu(ii) complexes synthesis, experimental and theoretical studies along with second-order nonlinear optical properties. *New Journal of Chemistry*, 2019, 43 (26), pp.10468-10481. 10.1039/c9nj01774g . hal-02278401

HAL Id: hal-02278401

<https://univ-rennes.hal.science/hal-02278401>

Submitted on 16 Sep 2019

HAL is a multi-disciplinary open access archive for the deposit and dissemination of scientific research documents, whether they are published or not. The documents may come from teaching and research institutions in France or abroad, or from public or private research centers.

L'archive ouverte pluridisciplinaire **HAL**, est destinée au dépôt et à la diffusion de documents scientifiques de niveau recherche, publiés ou non, émanant des établissements d'enseignement et de recherche français ou étrangers, des laboratoires publics ou privés.

Redox-Switching of ternary Ni(II) and Cu(II) complexes: Synthesis, experimental and theoretical studies along with second-order nonlinear optical properties^{†,‡}

Néstor Novoa,^{*a,b,c} Carolina Manzur,^b Thierry Roisnel,^c Vincent Dorcet,^c Nolwenn Cabon,^c Françoise Robin-Le Guen,^c Isabelle Ledoux-Rak,^d Samia Kahlal,^c Jean-Yves Saillard,^c David Carrillo^{*b} and Jean-René Hamon^{*c}

^a *Laboratorio de Química Inorgánica y Organometálica, Departamento de Química Analítica e Inorgánica, Facultad de Ciencias Químicas, Universidad de Concepción, Edmundo Larenas 129, Casilla 160-C, Concepción, Chile.
E-mail: nenovoa@udec.cl*

^b *Laboratorio de Química Inorgánica, Instituto de Química, Facultad de Ciencias, Pontificia Universidad Católica de Valparaíso, Avenida Universidad 330, Curauma, Valparaíso, Chile.
E-mail: David.carrillo@pucv.cl*

^c *Univ Rennes, CNRS, ISCR (Institut des Sciences Chimiques de Rennes) – UMR 6226, F-35000 Rennes, France.
E-mail: jean-rene.hamon@univ-rennes1.fr*

^d *Laboratoire de Photonique Quantique et Moléculaire, UMR CNRS 8537, ENS Paris Saclay, Institut d'Alembert, 61 Avenue du Président Wilson, 94235 Cachan Cedex, France.*

[†] Electronic supplementary information (ESI) available: CCDC 1901888-1901891. For ESI and crystallographic data in CIF or other electronic format see DOI:

[‡] This article is dedicated to our good friend and colleague Jean-François Halet on the occasion of his 60th birthday.

Abstract

Four new ternary Ni(II) and Cu(II) complexes of ONO tridentate Schiff base and pyridylmethylenepyran (PyMP) ligands [(R-ONO)M(PyMP)] (R = anisyl = An: M = Ni **1**, Cu **2**; R = ferrocenyl = Fc: M = Ni **3**, Cu **4**) have been synthesized under facile reaction conditions starting from R-ONOH₂, metal(II) nitrate salts, and PyMP; R-ONOH₂ stands for the Schiff base ligand precursors obtained by condensation of either 1-anisyl- or 1-ferrocenylbutan-1,3-dione and 2-aminophenol. They have been thoroughly characterized with the help of various physicochemical tools, such as CHN analyses, IR and UV-vis spectra, ¹H NMR for diamagnetic Ni(II) derivatives **1** and **3**, and HRMS for paramagnetic Cu(II) species **2** and **4**. The molecular structures of **1-3** were authenticated by single-crystal X-ray diffraction methods, along with that of the doubly phenoxide-bridged dimer [Cu₂(μ-ONO-Fc)₂(PyMp)₂] (**4'**), resulting from the recrystallization of **4**. In **1-3**, the four-coordinate nickel and copper atoms adopt a square planar geometry, whereas in **4'** the Cu^{II} metal ion is five-coordinated in a square pyramidal environment with the pyridyl nitrogen occupying the apex. Electrochemical studies reveal two well-separated redox waves. The spin density distribution analyses reveal that the initial oxidation process is associated with a ligand-based level, with some ferrocenyl participation for the heterobimetallic compounds **3** and **4**. Reversible redox switching can be established for **1** and **3** by time-resolved spectroelectrochemistry under thin-layer conditions where electrochemical cycling is associated with a significant modification of the UV-vis spectra of the chromophores. The second-order nonlinear optical responses of **1-4** along with those of assumed bispyrylium dimeric species **5** and **6**, generated by chemical oxidation of **1** and **3**, respectively, have been determined by harmonic light scattering measurements in dichloromethane solutions at 1.91 μm incident wavelength. Rather high β values ranging from 270 – 530 × 10⁻³⁰ esu were determined for **1-4**. β Value of **5** (800 × 10⁻³⁰ esu) was found to be almost twice that of its monomeric precursor **1**, whereas β value of **6** (160 × 10⁻³⁰ esu) is reduced by half with respect to that of **3**. In **5** the anisyl retains its donor ability whereas in **6** the electron-donating character of the oxidized ferrocenyl moiety is cancelled. Optimized geometries of the four compounds **1-4** as well as their electronic structures and that of their respective cations **1⁺-4⁺** have been analyzed through DFT calculations, while TD-DFT computation has been used to interpret the major features of the UV-vis spectra.

Introduction

The design and construction of new molecular architectures with variable dimensionality and different coordination frameworks exhibiting second-order nonlinear optical (NLO-2) properties have attracted considerable and continuous interest to prepare materials suitable for emerging optoelectronic and photonic technologies.¹ Molecules with high NLO-2 responses (molecular hyperpolarizability, β) must be non-centrosymmetric and possess strong electronic transitions of low energy and large variations of the dipole moment during the electronic excitation.² These properties can be accomplished by chromophores with a push-pull D- π -A type structure, containing both an electron-donor group (D) and an electron-acceptor group (A) linked through a π -conjugated system, which provides the polarizable electrons. In this regard, organic molecules with extensive π -delocalization were the focus of the most intense activity because of their ultrafast NLO-2 responses, good ability to be incorporated into thin-film devices, and enhanced non-resonant NLO-2 responses.³ When compared to organic molecules, organometallic complexes^{4,5} and coordination compounds^{6,7} represent a fascinating and growing class of second-order NLO chromophores that can offer additional flexibility, due to the presence of metal-ligand charge-transfer transitions, observed usually at relatively low-energy and high intensity, tunable by virtue of the nature, oxidation states, and coordination sphere of the metal centers. Those properties have been exploited to develop NLO-2 switches.⁸ The second-order NLO polarisabilities or first hyperpolarisabilities, may be changed by reversibly altering the electronic properties of the components of an NLO-active compound. On/off switching can be achieved by various external stimuli, such as chemical,⁹ electrical,¹⁰ optical^{8b,11} and redox^{8a,e,f,12} reactions. The first convincing demonstration of redox switching of NLO effects was reported by Coe et al. twenty years ago,¹³ on a system containing $[\text{Ru}(\text{NH}_3)_5]^{2+}$ as donor. Two years later, a reversible switching of the first hyperpolarisability of a NLO-active molecule containing the electroactive octamethylferrocene donor unit was also demonstrated.¹⁴ Since then, ferrocene has been extensively used in fine-tuning and switching the electronic properties of organometallic chromophores.¹⁵

During the last three decades, transition metal complexes of tri- and tetradentate Schiff base ligands¹⁶ have appeared as a promising class of efficient chromophores exhibiting good NLO responses, and are currently attracting considerable interest.¹⁷ Interest in those compounds comes from (i) their preparative accessibility and easy derivatization, (ii) their thermal stability, (iii) the active role, strategic position, and nature (closed-shell vs. open-

shell) of the metal ion which is a constituent of the polarizable bridge in the D- π -A structure, and (iv) the presence of charge transfer (CT) transitions at low energies. In this regard, we have recently designed a family of ternary square planar nickel(II) and copper(II) complexes of the type [(R-ONO)M(Py)], where R-ONO stands for a dianionic Schiff base ligand derived from the condensation of 2-aminophenol with either 1-anisyl- or 1-ferrocenyl -butan-1,3-dione, and Py is a pyridine based co-ligand. These four-coordinate Ni(II) and Cu(II) chromophores displayed good second-order NLO polarizabilities, with β values ranging from $170\text{-}350 \times 10^{-30}$ esu (HRS with $1.91 \mu\text{m}$ incident wavelength).¹⁸ In a more recent paper, we showed that the [(R-ONO)M] units can be used as building blocks for the construction of expanded and more complex architectures such as dimers and coordination polymers, taking advantage of the lability of the pyridine ancillary ligand.¹⁹ On the other hand, electrochemical studies have shown that the organic chromophores ferrocenyl-,²⁰⁻²³ pyridyl-,²¹ and phenyl-methylenepyrans²⁴ can undergo fast dimerization through C-C σ -bond making upon oxidation, and that the resulting bispyrylium species are irreversibly reduced back to the initial methylenepyran by C-C bond breaking. On the other hand, the first monomeric pyranyl-radicals have recently been isolated in the solid state, being prepared from redox-switchable carbene/pyrylium hybrids featuring three stable redox-states.²⁵ Pyrylium moieties act as chromophores and as such their non linear properties have been the subject of many studies, that are, for instance, relevant to all-optical signal processing,²⁶ or assessment of their potential as optical limiters²⁷

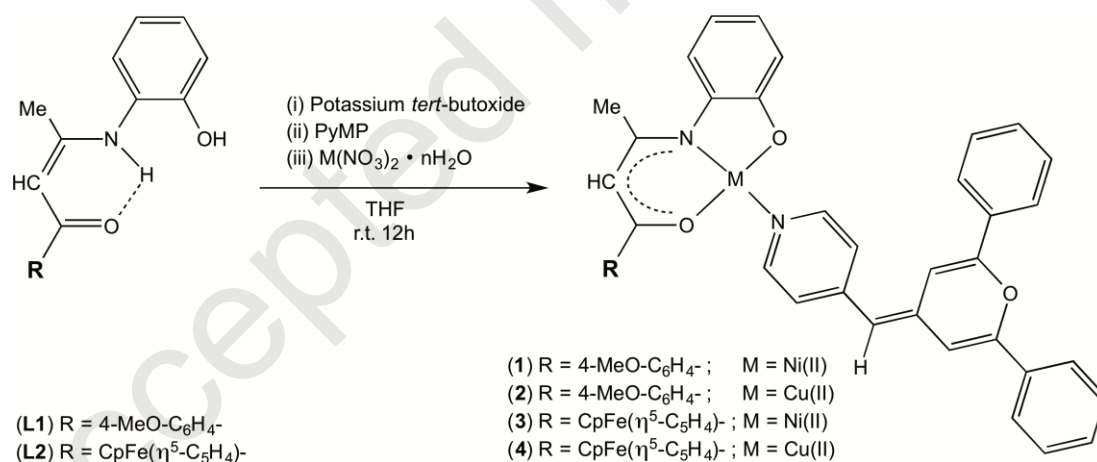
Interestingly, exchanging the labile pyridine ligand by its pyridylmethylenepyran (PyMP) counterpart would lead to the formation of new chromophoric complexes of the type [(R-ONO)M(PyMP)] that could exhibit redox-triggered switching of NLO-2 response *via* dimerization of chemically or electrochemically generated radical cations. In this contribution, we report on the synthesis, analytical and spectral characterization of the four neutral ternary mononuclear and heterobimetallic complexes [(R-ONO)M(PyMP)] (R = anisyl (An): M = Ni, **1**; Cu, **2**; R = ferrocenyl (Fc): M = Ni, **3**; Cu, **4**) (see formulas in Scheme 1). The crystal and molecular structures of compounds **1-3**, as well as that of the doubly phenoxide-bridged dimer [Cu₂(μ -Fc-ONO)₂(PyMP)₂] (**4'**) have been determined by single crystal X-ray diffraction analysis. Redox properties were investigated for all the complexes, and spectroelectrochemical experiments were carried out to characterize the switching properties of the two Ni(II) derivatives **1** and **3** by variation of the applied potential. The nonlinear optical properties of **1-4** and those of compounds **5** and **6** generated by chemical oxidation of **1** and **3**, respectively, have been determined using the Harmonic Light Scattering

(HLS) technique. In addition, DFT and its time-dependent DFT extension (TD-DFT) provide a rationalization of the structural, electrochemical, spectroscopic and optical properties.

Results and discussion

Synthesis and characterization of complexes

The mononuclear (**1**, **2**) and bimetallic (**3**, **4**) complexes were readily prepared by reacting the known tridentate Schiff-base ligand precursors R-C(O)CH=C(CH₃)NH-C₆H₄-2-OH (R = anisyl (**L1**), ferrocenyl(**L2**))¹⁸ with one equiv. of hydrated M(II) nitrate salt (M = Ni, Cu), and a slight excess of the electro-active pyridyl 2,6-diphenylmethylenepyran (PyMP), under basic conditions in THF for 12 h at room temperature (see Experimental for details and Scheme 1). Compounds **1-4** were isolated as light-brown microcrystalline powders in 72-75% yield. Single crystals suitable for X-ray diffraction study (see below) were obtained for each complex by recrystallization from dichloromethane dissolutions. Derivatives **1-4** are air and thermally stable and moisture insensitive on storage under ordinary conditions. They exhibit very high solubility in common polar organic solvents but are not soluble in diethyl ether and others nonpolar hydrocarbons.



Scheme 1. Synthesis of complexes **1-4**.

Satisfactory elemental analyses, FT-IR, 1D and 2D NMR experiments (for diamagnetic nickel(II) species **1** and **3**), UV-vis spectroscopy, and single-crystal X-ray diffraction study established the purity, composition and identity of the four compounds. In addition, positive mode electro spray ionization mass spectrometry (ESI⁺-MS) confirms the molecular composition of the paramagnetic Cu(II) complexes **2** and **4** with well detectable [M]⁺ ion peaks at m/z (a.u.) = 667 and 745, respectively (see Experimental). The fragment

peak $[\text{PyMP} + \text{H}]^+$ at m/z (a.u.) = 324 is also observed in both spectra, as well as the fragment peak $[\text{M} - \text{PyMP}]^+$ at m/z (a.u.) = 422 in the mass spectrum of **4**.

In the solid-state FT-IR spectra of **1-4**, the O-H and N-H absorption bands observed in the spectra of their two Schiff base ligand precursors vanished, thus indicating that the coordination of the $[(\text{R-ONO})]^{2-}$ ligand to the metal(II) ion has taken place through both deprotonated oxygen and nitrogen atoms. Moreover, the presence of characteristic strong intensity bands in the range $1645\text{-}1495\text{ cm}^{-1}$, assigned to the stretching vibrations of the $[\text{O}=\text{C}-\text{C}=\text{C}=\text{N}]$ Schiff base skeleton, confirms the coordination of the imine nitrogen and of the carbonyl oxygen atoms. The strong band at 1240 and 1256 cm^{-1} for **1** and **2**, respectively, are assigned to the ν_{asym} vibration mode of the $\text{CH}_3\text{-O-C}_6\text{H}_4$ group. The $\nu(\text{C}=\text{C})$ stretching vibrations of the PyMP fragment, showing up in the range $1504\text{-}1408\text{ cm}^{-1}$, could only be observed for the bimetallic species **3** and **4**. Lastly, the deformation modes of the C-H vibration were seen for the four compounds in the $753\text{-}770\text{ cm}^{-1}$ region.

^1H NMR spectra were recorded for the two diamagnetic Ni(II) species **1** and **3**, and displayed the expected resonance patterns consistent with the proposed structures (see Experimental section for complete assignments). In **1**, the Schiff base ligand showed three sharp singlets at δ_{H} 2.49, 3.73, and 5.22 with integral ratio 3:3:1, attributed to the methyl, methoxy, and methine protons, respectively. In **3**, the ferrocenyl-containing Schiff base ligand gives rise to a similar peak pattern with integral ratio 3:5:1 for the protons of the methyl, free cyclopentadienyl ring, and methine groups resonating at δ_{H} 2.45, 4.09, and 5.50, respectively. In both **1** and **3**, the three magnetically nonequivalent protons of the $-\text{CH}=\text{C}_5\text{H}_2\text{O}$ fragment of the PyMP ligand gave rise to three separate resonances at δ_{H} 5.81 and 5.74 (H-23 and H-26), 6.98 and 6.44 (H-28 and H-31), and 7.18 and 7.02 (H-25 and H-28), respectively (see Chart S1 for the numbering schemes, ESI[†]). The *ortho* protons of the pyridyl units appeared at δ_{H} 8.44 (H-18, 22) for **1** and 8.41 (H-21, 25) for **3**, as the most downfield shifted ones in both spectra. With respect to the chemical shifts of the free PyMP ligand, those of the *ortho* protons as well as those of the exocyclic $-\text{CH}=\text{C}$ protons (H-23 and H-26) are barely affected ($\delta_{\text{H}} < 0.10$) by its complexation to the Ni(II) center.²¹

The ionic derivatives **5** and **6** were instantaneously generated as brown and dark red solids, by chemical oxidation upon treatment of their Ni(II)-containing precursors **1** and **3** with one and two equivalents of AgPF_6 , respectively, in dichloromethane : MeOH (2:1, $v:v$) mixture at room temperature (Scheme S1, ESI[†]). Albeit they could only be partially characterized by their solid-state FT-IR spectroscopy, they were assigned a dimeric

bispyrylium-type structure based on our previous works.²⁰⁻²⁴ Their IR spectra exhibited characteristic absorption bands of the [O=C=C=C=N] Schiff base ligand skeleton in the range 1650-1600 cm⁻¹, as well as strong and medium intensity bands at 852/551 and 845/542 cm⁻¹, respectively, due to the PF₆⁻ anions. Owing to their low stability, they were immediately used for NLO measurements (see below).

Description of the X-ray crystal structures

Single crystals suitable for X-ray structure investigation were obtained for the four complexes by slow evaporation of their corresponding dichloromethane solution (see Experimental). Complex **4** crystallizes as its doubly phenoxo-bridged dimer that will be denoted as **4'** (see Scheme S2, ESI[†]). Fig. 1 displays pictorial views of discrete mononuclear and bimetallic units of **1** and **3**, respectively, and that of the tetrametallic complex **4'** is shown in Fig. 2.

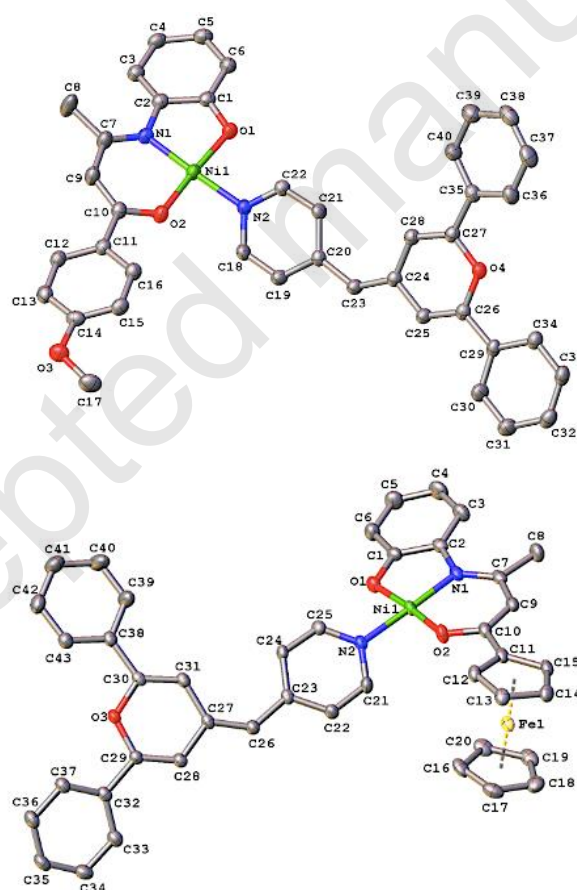


Fig. 1 Molecular structures of the mononuclear complex **1** (top) and of the bimetallic species **3** (bottom) showing the atom labelling scheme. Hydrogen atoms have been omitted for clarity. Thermal ellipsoids are drawn at 30 and 40% probability, respectively.

The molecular structure of **2**, isostructural of **1**, is presented in Fig. S1 (ESI[†]). Selected bond distances and angles for the first M(II) coordination sphere (M = Ni, Cu) of compounds **1-3** and **4'** are gathered in Tables 1 and 2, respectively. Additionally, selected bond distances and angles for the ligands in **1** and **2**, and in **3** and **4'** are listed in Tables S1 and S2, respectively (see ESI[†]). The single-crystal X-ray diffraction studies confirm that in each compound, the metal ion (either Ni(II) in **1** and **3**, or Cu(II) in **2** and **4'**) is chelated by the dianionic [R-ONO]²⁻ tridentate Schiff base ligand, and that the PyMP ligand coordinates to the metal center through the nitrogen atom of the pyridyl unit. In **3** and **4'**, the ferrocenyl unit features a typical linear η^5 -Fe- η^5 sandwich structure, with metrical parameters in agreement with a Fe(II) oxidation state in the metallocenyl units (Table S3, ESI[†]). The cyclopentadienyl rings are parallel and eclipsed. On the pyridylmethylenepyran side, the exocyclic C-C bond lengths lie in the range 1.364(3) - 1.377(8) Å (Tables S1 and S2, ESI[†]), in agreement with previous reports and suggesting a weak pyrylium character.^{21,23} The other aspects of the structures are discussed below in two sections for the sake of simplicity.

Compounds 1-3. Both mononuclear Ni(II) **1** and bimetallic Ni(II)/Fe(II) **3** derivatives crystallize in the monoclinic centrosymmetric space groups P2₁/n and P2₁/c, respectively. The mononuclear Cu(II) complex **2** crystallizes in the orthorhombic non-centrosymmetric space group P2₁c. The asymmetric unit of each complex contains one molecule. In the three complexes, the centered M(II) ion is tetracoordinated, bonded to the imine nitrogen atom and to the carbonyl and phenolato oxygen atoms of the chelating Schiff base ligand, and to the nitrogen atom of the pyridylmethylenepyran co-ligand (Figs. 1 and S1, ESI[†]). In **1** and **3**, the nickel center adopts a slightly distorted square planar geometry that is more distorted at the Cu(II) metal ion in **2**. In the three cases, the nitrogen and oxygen atoms occupy mutually *trans* dispositions with diagonal angles ranging from 174.74(8)° to 176.69(9)° in **1** and **3**, and of 168.5(2)° and 170.4(2)° in **2**, strongly deviating from linearity in this latter case (Table 1).

The extent of deformation in a tetracoordinated complex can be quantified by the four-coordinate geometry τ_4 index.²⁸ This parameter, which measures the extent of distortion between a perfect square planar geometry ($\tau_4 = 0$) and a perfect tetrahedral geometry ($\tau_4 = 1$), is obtained by the formula: $\tau_4 = [360 - (\alpha + \beta)]/141$, α and β being the two largest bond angles of the metal coordination sphere. The Ni(II) complexes **1** and **3** have a τ_4 values of 0.058 and 0.063, respectively, over 0.150 for the Cu(II) counterpart **2**. The central Ni(II) atoms barely deviate from the ONON basal plane by 0.013(1) and 0.015(1) Å, respectively, while the

deviation is more significant for the Cu(II) atom (0.154(4) Å). Consequently, the angular summations of 361.9° measured for the Cu(II) complex **2** slightly departs from the idealized value of 360.0° found for the two Ni(II) derivatives **1** and **3**.

The bond lengths and angles in the first coordination sphere of the centered metal ions in **1-3** (Table 1) are very similar to those measured for their respective parent complexes,¹⁸ the M-N(2) bond distances being always the larger ones. The fused five- and six-membered heterometallacycles formed upon chelation of the Ni(II) and Cu(II) metal ions are essentially co-planar. In **1**, the anisyl substituent makes a dihedral angle of 20.2(1)° with the plane of its attached heterometallacycle while both planes are almost co-planar (3.4(4)°) in the Cu(II) congener **2**. This dihedral angle is of 17.6(1)° with the substituted cyclopentadienyl ring in **3**. The pyridyl unit of the PyMP ligand is twisted by 38.4(1)°, 18.7(2)° and 35.3(1)°, respectively, with respect to the metal coordination plane. In addition, the O-C, C-C and C-N bond falling between single and double bond lengths and bond angles of sp² hybridized atoms (Tables S1 and S2, ESI[†]), suggests a significant electron delocalization throughout the entire heterometallacycles framework.

Table 1. Selected X-ray and DFT-optimized (into square brackets) bond distances (Å) and angles (°) for the first metal(II) coordination sphere of compounds **1**, **2** and **3**.

	1	2	3
Bond distances			
M(1)-O(1)	1.8300(18) [1.838]	1.909(4) [1.915]	1.8218(18) [1.838]
M(1)-O(2)	1.8236(18) [1.838]	1.893(5) [1.919]	1.8191(18) [1.841]
M(1)-N(1)	1.874(2) [1.880]	1.945(5) [1.961]	1.884(2) [1.880]
M(1)-N(2)	1.918(2) [1.932]	1.999(6) [2.024]	1.927(2) [1.932]
Bond angles			
O(1)-M(1)-O(2)	175.17(8) [176.9]	170.4(2) [179.0]	174.74(8) [176.7]
N(1)-M(1)-N(2)	176.69(9) [175.9]	168.5(2) [176.0]	176.30(9) [175.4]
O(1)-M(1)-N(1)	87.36(9) [86.9]	85.8(2) [85.0]	88.01(8) [86.9]
O(1)-M(1)-N(2)	89.49(8) [89.1]	92.5(2) [91.1]	88.54(8) [89.0]
O(2)-M(1)-N(1)	96.75(9) [96.1]	94.3(2) [94.1]	97.19(9) [96.2]
O(2)-M(1)-N(2)	86.44(8) [87.9]	89.2(2) [90.0]	86.28(8) [88.0]

M = Ni, 1 and 3; Cu, 2.

Tetrametallic complex 4'. The dimeric species **4'** crystallizes in the triclinic centrosymmetric space group P-1 with half a molecule in the asymmetric unit. Compound **4'** consists of a centrosymmetric bis(μ -phenoxo)di-copper(II) complex with the two halves of the dimeric unit related by a crystallographic inversion center in the middle of the four membered Cu_2O_2 core (Fig. 2). This antisymmetric rhombus exhibits two distinct bridging Cu-O bond lengths of 1.946(2) and 1.980(2) Å (Table 2). The Cu-O-Cu bridge angle is of $103.21(9)^\circ$, and the two copper atoms are separated by 3.077(3) Å. All these bond distances and angles are in good agreement with those recently reported for analogous doubly phenoxo bridged square pyramidal Cu(II) species.^{19,29}

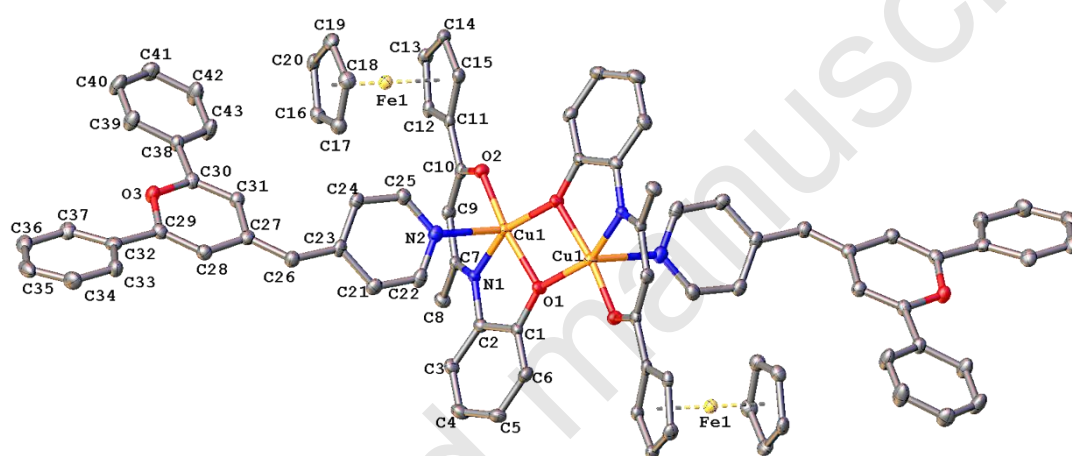


Fig. 2 Molecular structure of the dimeric tetra-metallic complex **4'** showing the atom labelling scheme. Hydrogen atoms have been omitted for clarity. Thermal ellipsoids are drawn at 40% probability. Half unit of complex **4'** was generated by symmetry operations $-x$, $-y$, $-z$.

In **4'**, each pentacoordinated Cu(II) center adopts a square pyramidal coordination geometry with the basal plane formed by the ONO donor set of the ferrocenyl-containing Schiff base ligand and the bridging oxygen atom of the second half-unit. The apical site is occupied by the nitrogen atom of the PyMP ligand. This arrangement of donor atoms around the metal center is somewhat different from that found in the related dimer $[\text{Cu}_2(\text{An-ONO})_2(\text{Py}^*)_2]$ in which Py^* is the 4-*tert*-butylpyridine.²⁹ In that case, the basal plane about the first Cu(II) center consists of a N_2O_2 donor set while the apical site is occupied by the bridging phenoxido oxygen atom of the ONO-tridentate ligand that is basal to the second Cu(II) ion of the dimer. The trigonality index (τ), known as Addison's parameter,³⁰ is used to quantify the distortion from the square-pyramidal ($\tau = 0$) to the trigonal-bipyramidal ($\tau = 1$)

geometry, is calculated to be 0.03, indicating that the geometry around the five-coordinate Cu(II) center reaches an almost idealized square pyramid. The copper atom moves away from the basal plane by 0.178(1) Å due to the formation of the axial bond. This Cu(1)-N(2) axial bond length (2.418(3) Å) is much longer than the equatorial one (1.948(3) Å), but similar to the Cu-O axial bond length (2.445(3) Å) measured in [Cu₂(An-ONO)₂(Py*)₂].²⁹

The bond distances of the donor atoms of the tridentate Schiff base ligand to the central copper atom in **4'** (Table 2) are similar to those measured in the mononuclear species **2** (Table 1), and are in agreement with literature data.^{7d,18,19,31} As depicted above for **1-3**, the fused five- and six-membered heterometallacycles in **4'** are also essentially co-planar, being also almost co-planar with the cyclopentadienyl ring (dihedral angle = 5.0(2)°). Such a flatness along with interatomic distances and angles (Tables S2, ESI[†]) are indicative of substantial π -delocalization of the electron density over the entire Schiff base ligand.

Table 2. Selected X-ray bond distances (Å) and angles (°) for the first Cu(II) coordination sphere of compound **4'**.

Bond distances			
Cu(1)-N(1)	1.948(3)	Cu(1)-N(2)	2.418(3)
Cu(1)-O(1)	1.946(2)	Cu(1)-O(2)	1.883(2)
Cu(1)-O(1) ^{#1}	1.980(2)	Cu(1)-Cu(1) ^{#1}	3.077(3)
Bond angles			
O(1)-Cu(1)-O(2)	170.63(9)	O(1)-Cu(1)-N(1)	83.76(9)
O(1)-Cu(1)-O(1) ^{#1}	76.79(9)	O(1)-Cu(1)-N(2)	96.52(9)
N(1)-Cu(1)-O(2)	97.84(10)	N(1)-Cu(1)-N(2)	91.24(10)
N(1)-Cu(1)-O(1) ^{#1}	157.78(10)	O(2)-Cu(1)-N(2)	92.68(9)
O(2)-Cu(1)-O(1) ^{#1}	99.67(9)	N(2)-Cu(1)-O(1) ^{#1}	101.46(9)

Symmetry transformations used to generate equivalent atoms: #1 -x+1,-y+1,-z+2

Electrochemical and spectroelectrochemical studies

The redox behavior of the new compounds **1-4** was investigated by cyclic voltammetry in dichloromethane containing [*n*-Bu₄N][PF₆] (0.1 M) as supporting electrolyte, in the potential range -2.50 – 1.20 V vs. FcH/FcH⁺. Compounds **1-4** were not reducible in this electrochemical window. All potentials are quoted versus the FcH/FcH⁺ redox couple. The redox behavior of **1-4** is quite similar to that of their parent complexes [(R-ONO)M(py)].¹⁸ That is two irreversible waves for the M(II)-centered mononuclear species **1** and **2**, and a

reversible (or quasi-reversible) redox process followed by a broad irreversible one for the ferrocenyl-containing derivatives **3** and **4**. Interestingly, the redox potentials of **1-4** are cathodically shifted by about 150 mV with respect to those of their parent counterparts.³² The lowering of the oxidation potential may be explained by better electron donating ability of the PyMP ligand compared to pyridine.

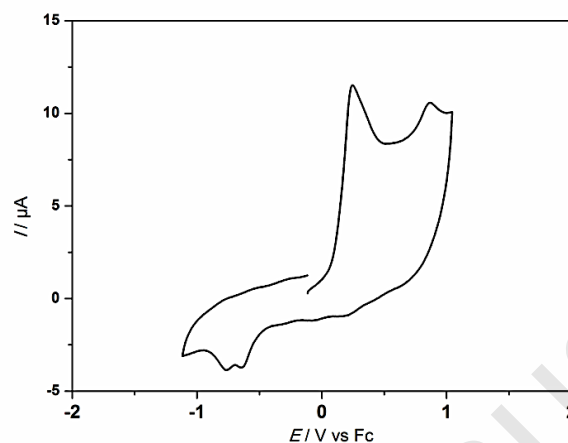


Fig. 3 Cyclic voltammogram of compound **1** (1 mM) in $\text{CH}_2\text{Cl}_2/[\textit{n}\text{-Bu}_4\text{N}][\text{PF}_6]$ (0.1 M), $\nu = 0.1 \text{ Vs}^{-1}$, Pt disk working electrode.

As stated above, both compounds **1** (Fig. 3) and **2** (Fig. S2, ESI[†]), exhibit two irreversible monoelectronic anodic waves in their respective cyclic voltammogram. The first oxidation peaks observed at $E_p^{\text{ox}1} = 0.27 \text{ V}$ and 0.14 V , respectively, are attributed to ligand-based redox process (see the Theoretical Investigations section below).³³ Usually, for organic derivatives containing the methylenepyran group, an irreversible oxidation, localized on the methylenepyran part of the molecule, is observed around $E_p^{\text{ox}} = 0.2\text{-}0.8 \text{ V vs. FcH/FcH}^+$.³⁴ The second oxidation waves at $E_p^{\text{ox}2} = 0.92 \text{ V}$ and 0.89 V could be tentatively assigned to the Ni(II)/Ni(III) and Cu(II)/Cu(III) redox couples, respectively.¹⁸ Additionally, in the case of **1**, a study of the cyclic voltammogram at different scan rates shows that whereas the ratio $i_p^{\text{ox}1}/\nu^{1/2}$ is constant for the first oxidation, it tends to decrease at slower scan rates for the second oxidation, indicating a competition between the second electron transfer and a chemical reaction following the first electron transfer, (EC process).³⁵

In the case of the ferrocenyl-containing compounds **3** and **4**, the first oxidation at $E_p^{\text{ox}1} = 0.05 \text{ V}$ and 0.07 V (Figs. S3 and S4, ESI[†]), respectively, was found to be monoelectronic and *quasi*-reversible. This electrochemical behaviour is similar to that observed with the parent compounds $[(\text{Fc-ONO})\text{M}(\text{py})]$,¹⁸ and might be associated with the oxidation of the ferrocenyl moiety. Our DFT calculations suggest also ligand oxidation, with some ferrocenyl

participation (see below). Moreover, this first oxidation process is followed by a broad but well-defined wave at $E_p^{\text{ox}2} = 0.40$ and 0.44 V, respectively, probably merging two very close successive oxidations that could be related to consecutive ligand based oxidation processes with a possible participation of iron and M(II).^{18,24,33}

Our interest in the incorporation of the PyMP ligand into complexes **1-4** focused on the fact that under electrochemical oxidative stimuli the methylenepyran fragment was likely to dimerize into bispyrylium species, which in turn could be reduced back to the initial methylenepyran compound. This reversible electron-induced C-C making/breaking bond was already studied by our group,^{20,22,36} and others.³⁷ Recently, we have conducted a spectroelectrochemical study on a series of phenylmethylenepyran organic molecules where the phenyl group was substituted at the *para*-position by different groups R (R = H, Br, NO₂, CO₂Me, NMe₂, OMe).²⁴ Under oxidation and depending on the nature of the R group, a 20-50 nm red-shift of the absorption band at 350-400 nm (except for R= NO₂) was observed on the UV-visible absorption spectra, corresponding to the formation of the bispyrylium species. In the meantime, an irreversible reduction peak, characteristic of the bispyrylium species, was therefore detected around -0.8 V vs FcH/FcH⁺ by thin layer cyclic voltammetry (TLCV). This process was reversible since the reduction of the bispyrylium species led back to the initial cyclic voltammogram and to the initial UV-visible spectrum.²⁴

For this work, we decided to conduct a similar spectroelectrochemical study on the two nickel(II) coordination derivatives **1** and **3** to see if a reversible process could be reached. The cyclic voltammetry of **1** was realized under thin layer conditions (TLCV), and shows one oxidation peak and two peaks in reduction on the backward scan (Fig. 4(A)). During the cycling, the UV-visible spectrum was recorded and showed the appearance of two new bands at 331 nm and 493 nm under oxidation whereas the intensity of the band at 419 nm decreases (Fig. 4(B)), which implies a bathochromic shift of 74 nm under oxidation. When the scan of the cyclic voltammetry was completed, the initial UV-visible spectrum was recovered, suggesting a reversible overall redox process.

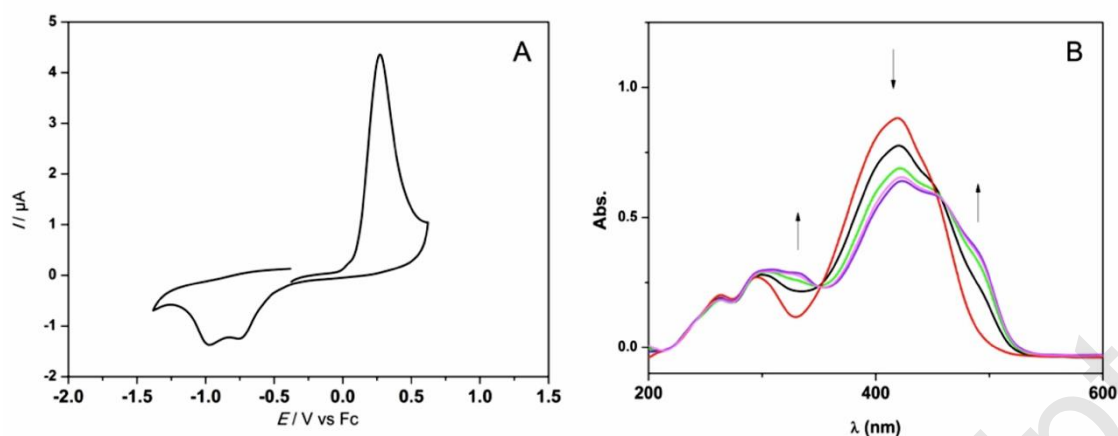


Fig. 4 (A) TLCV of **1** ($C = 1.3 \text{ mM}$) in $\text{CH}_2\text{Cl}_2/[n\text{-Bu}_4\text{N}][\text{PF}_6]$ (0.1 M), $v = 5 \text{ mVs}^{-1}$, Pt disk, and (B) Evolution of the UV-visible spectrum of compound **1** during its oxidation by TLCV.

In the case of the bimetallic complex **3**, two successive oxidations occurred by TLCV and when the scan was done until the second oxidation, a variation of the UV-visible spectrum comparable to the one observed for **1** was noticed (Fig. S5, ESI[†]). Indeed, two new bands at 326 nm and 494 nm increase and the decrease of the band at 420 nm was noted. Then, a bathochromic shift of 74 nm under oxidation was also determined. A complete return to the initial UV-visible spectrum was only observed when the back scan was done until the second reduction as for complex **1**. Adding to the fact that after a few scans the shape of the CV remained unchanged, these preliminary results suggest the occurrence of a reversible oxidation/reduction process.

On the basis of our previous study, the process could imply a dimerization (C-C bond formation) under oxidation and a C-C bond cleavage during the reduction process, but at this point of the study, we do not have enough information to describe the entire electrochemical process. In order to get more information on the oxidation product, exhaustive electrolysis of solutions of **3** after the second oxidation ($0.8 \text{ V vs FcH/FcH}^+$) was attempted, but no stable product could be isolated on the electrolysis timescale. A chemical oxidation of **1** and **3** with an oxidizing agent (AgPF_6) was also attempted (see above). Unfortunately, because of the low solubility of the product, it was not possible to prove the formation of a dimer (by cyclic voltammetry).

Electronic absorption spectra

The electronic absorption spectra in the UV-visible region for compounds **1-4** were measured in CH₂Cl₂ solutions, showing a well-defined low-energy band at ~ 400 nm, a less marked peak or shoulder at ~ 290 nm and a high-energy band split into two close extrema around 230-250 nm (see Fig. 5, Table 3 and Fig.S6, ESI[†]). The close similarities between the four spectra suggest that they are dominated by ligand-to-ligand transitions, the metal atoms playing a minor role in the observed transitions. This is confirmed by our TD-DFT results (see below).

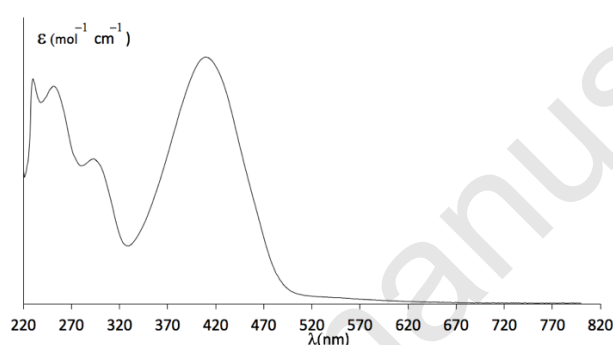


Fig. 5 Experimental UV-vis absorption spectrum of **1** recorded in CH₂Cl₂ solution at 20 °C.

Table 3 UV-vis absorption data for compounds **1-4** (left columns: experimental λ_{\max} (nm) with associated $\log(\epsilon)$ in parentheses; right columns: computed major transitions (nm) associated with the lowest absorption bands and their associated oscillator strengths in parentheses).

1		2		3		4	
Exp.	Calc.	Exp.	Calc.	Exp.	Calc.	Exp.	Calc.
253 (3.83)	-	256 (3.77)	-	246 (3.79)	-	245 (3.87)	-
294 (3.66)	311 (0.36) H-5→L $\pi(\text{Ph})\rightarrow\pi^*(\text{Py})$	285 (3.73)	310 (0.35) H-7→L $\pi(\text{Ph})\rightarrow\pi^*(\text{Py})$	290 (3.50)	311 (0.36) H-7→L $\pi(\text{Ph})\rightarrow\pi^*(\text{Py})$	281 (3.67)	-
410 (3.89)	410 (1.12) H-1→L $\pi\rightarrow\pi^*(\text{PyMP})$	399 (3.85)	409 (1.28) H-1→L $\pi\rightarrow\pi^*(\text{PyMP})$	408 (3.80)	409 (1.26) $\pi\rightarrow\pi^*(\text{PyMP})$	397 (3.83)	409 (1.26) $\pi\rightarrow\pi^*(\text{PyMP})$

Quadratic Nonlinear Optical Studies

The quadratic nonlinear responses of the neutral compounds **1-4** and of the ionic species **5** and **6** have been determined at 1.91 μm incident wavelength using the HLS technique (see Experimental for details). The HLS measurements were carried out in dichloromethane solutions for all the compounds. The experimental β values are gathered in Table 4.

Table 4 HLS β values determined at λ_{inc} 1.91 μm for compounds **1-6**.^a

Compd ^b	β (10^{-30} esu)
1	530
2	270
3	330
4	340
5	860
6	160

^aRelative experimental error on β value is $\pm 10\%$.

^b 10^{-2} M solution in CH_2Cl_2 .

It is interesting to note that the qualitative behavior of compounds **1-4** is similar to that of their respective [(R-ONO)M(Py)] counterparts bearing the pyridine (Py) co-ligand.¹⁸ That is a higher β value for the mononuclear Ni(II) complex **1** than for its Cu(II) congener **2** and, within the 10% experimental error, equivalent β values for the heterobimetallic species **3** and **4** (Table 4). However, β values found for **3** and **4** are two-fold greater than those determined for their corresponding [(Fc-ONO)M(Py)] derivatives ($\beta = 170 \times 10^{-30}$ esu). Surprisingly, the second-order NLO response of the Ni(II) complex **1** is also twice that of its Cu(II) homologue **2** (Table 4). It is possible that the significant distortion of copper complexes as compared to nickel-based ones weakens the intramolecular charge transfer (ICT) between the anisyl donor group and the electro-attractive part of the complex.

The strong decrease of β for the heterobimetallic complex **3** with respect to the mononuclear derivative **1** (Table 4) is similar to that observed in the [(R-ONO)Ni(Py)] series.¹⁸ If we calculate the non-resonant “static” $\beta(0)$ values from the experimental one measured at 1.91 μm using a two-level dispersion model,³⁸ we find $\beta(0) = 340 \times 10^{-30}$ esu for

1 and $\beta(0) = 270 \times 10^{-30}$ esu for **3**. The remaining difference between **1** and **3** can be assigned to the different natures of their respective R substituents, the anisyl group bringing more π -electrons to the conjugated chain of the ligand than the ferrocenyl one. In addition, steric constraints could also favor this decrease of β by generating a substantial twisting of the ferrocenyl moieties that may be a barrier to efficient ICT.

The strong increase of β values on passing from **1** to its dicationic counterpart **5** can be assigned to the oxidation-induced dimerization of the monomeric unit **1**, concomitantly generating the electron-withdrawing chromophoric bispyrylium moiety. In principle, dimerization should qualitatively increase the β value, but more information about the symmetry of compound **5** would be necessary to quantitatively evaluate this contribution. Another factor influencing the first hyperpolarizability, β , would be the modification of the intramolecular charge transfer due to the oxidation process. Anyway, oxidation does not appear to weaken significantly the ICT, then resulting in a high β for compound **5**. On the other hand, the strong decrease of β value for compound **6** with respect to **3** is due to the cancellation of the electron-donating character of the oxidized ferrocenyl moiety, a phenomenon that does not appear in complex **5** where the anisyl donor group is not oxidized.

Theoretical investigations

DFT calculations were performed on compounds **1-4** (see Computational details in the Experimental section). Their fully optimized geometries are in good agreement with the X-ray structures of **1-3** (see Tables 1 and 2, S1 and S2 ESI[†]). The Kohn-Sham orbital diagrams of **1** and **3** are given in Fig. 6. The four highest occupied orbitals of the 16-electron complex **1** are of major ligand character: Schiff base (HOMO and HOMO-2) PyMP (HOMO-1) and anisyl (HOMO-3). The highest occupied level of dominant Ni character is the HOMO-4. The lowest unoccupied level of dominant Ni character (antibonding $d_{x^2-y^2}$ orbital) is the LUMO+1. The LUMO is PyMP-centered, as well as the LUMO+2. Going from **1** to **3**, corresponds to the introduction of three “ t_{2g} -type” Fe occupied orbitals as the HOMO-2, HOMO-3 and HOMO-4. The LUMO and LUMO+3 are similar, whereas the LUMO+1 and LUMO+2 are switched. In addition, the LUMO+2 of **3** has gained 17% of Fc participation. Thus, except for their Ni($d_{x^2-y^2}$) LUMO+2 (in **3**) orbital, the frontier orbitals of **1** and **3** have no important metal character. The Kohn-Sham spinorbital diagrams of **2** and **4** (Fig. S7, ESI[†]) are more or less related to that of **1** and **3**, although more complex due to spin polarization. In these two 17-electron complexes, the Cu($d_{x^2-y^2}$) single electron is associated with a rather low-lying

occupied α spinorbital and a second lowest vacant β spinorbital. The spin density plots of **2** and **4** (Fig. 7) indicate clearly its Cu-ligand antibonding nature.

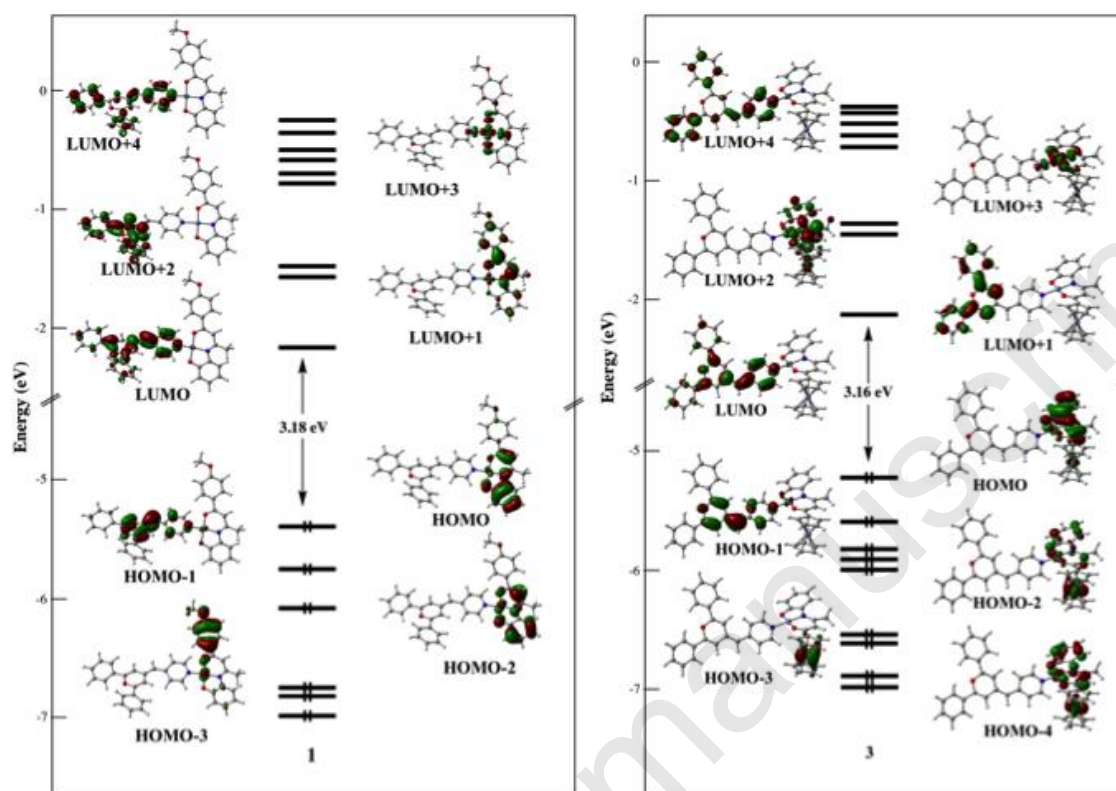


Fig. 6 Kohn-Sham orbital diagrams of **1** and **3**.

Calculations on $\mathbf{1}^+$ and $\mathbf{3}^+$ indicate that the one-electron oxidation of **1** and **3** corresponds to the removal of an electron to their Schiff base-centered HOMO and Fe-centered HOMO-2, respectively, as illustrated by the spin density plots of the $\mathbf{1}^+$ and $\mathbf{3}^+$ cations shown in Fig. 7. The ground states of $\mathbf{2}^+$ and $\mathbf{4}^+$ were found to be triplets. It turns out that the one-electron oxidation of **2** and **4** does not correspond to the removal of the Cu($d_{x^2-y^2}$) single electron, but rather to a ligand-based level, as in **1**. Thus, the spin density reflects the localization of one single electron in the Cu($d_{x^2-y^2}$) orbital (as in **2** or **4**) and another one on the ligand (as in $\mathbf{1}^+$). In the case of $\mathbf{4}^+$, one can note a minor Fe participation to the spin density.

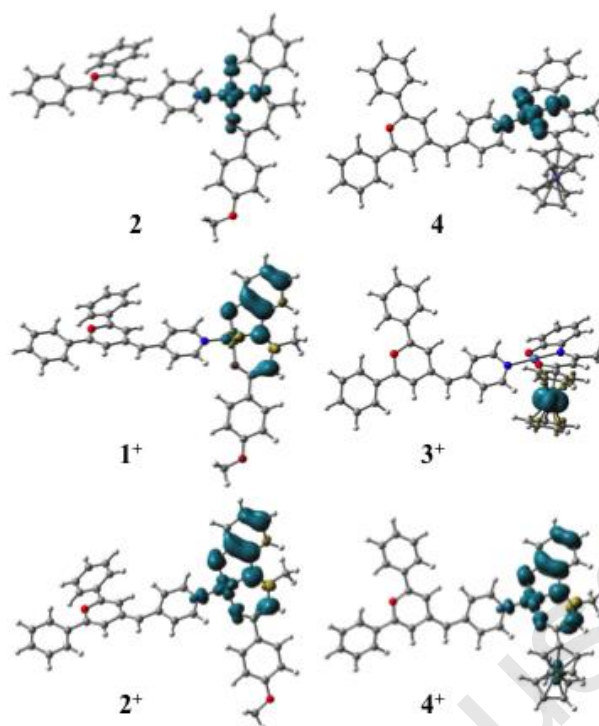


Fig. 7 Computed spin densities of the ground states of **2**, **4** and **1⁺-4⁺**.

TD-DFT calculations were performed on compounds **1-4** (see Table 3) in order to index their optical transitions of lowest energy. For the sake of computational cost, only the two lowest bands were indexed for **1-3** and the lowest one for **4** (see Table 3). The computed and experimental values are in very good agreement. For the four compounds, the band of lowest energy is mainly associated with a HOMO-1→LUMO character, *i.e.* to a PyMP $\pi \rightarrow \pi^*$ intraligand transition. The next absorption feature is associated with a transition involving a low-lying level of large phenyl character and the LUMO, thus also an intraligand transition, with significant phenyl \rightarrow pyridyl charge transfer. Although the transitions of higher energy were not computed, our TD-DFT results confirm the above-mentioned suggestion that the UV-vis spectra are dominated by ligand-to-ligand transitions.

Conclusions

In summary, this paper describes the synthesis of a series of mono-, bi- and tetrametallic nickel(II) and copper(II) complexes with chelating ONO-tridentate Schiff base and pyridylmethylenepyran ligands of the type [(R-ONO)M(PyMP)], and their full characterization by a number of physicochemical techniques. Their molecular structures have been determined by single crystal X-ray diffraction analysis. Both the mononuclear Ni(II) and Cu(II) complexes [(An-ONO)M(PyMP)] as well as the heterobimetallic derivative [(Fc-ONO)Ni(PyMP)] form discrete molecular entities in which the four-coordinate central metal(II) ion sits in a square planar environment. By contrast, the heterobimetallic complex [(Fc-ONO)Cu(PyMP)] crystallizes as a doubly phenoxide-bridged dimer [Cu₂(μ-ONO-Fc)₂(PyMP)₂], exhibiting two penta-coordinated Cu(II) centers with a square pyramidal N₂O₃-coordination sphere. The two halves of the dimer are related through a planar Cu₂O₂ rhombic core. Geometry, bonding, electronic structure and electrochemical properties have been rationalized by DFT calculations. Indexation of the optical transitions was supported by TD-DFT computation, confirming that the UV-vis spectra are dominated by ligand-to-ligand transitions. Time-resolved spectroelectrochemical experiments under thin-layer conditions have been carried out with the two Ni(II) complexes. Recovery of initial UV-vis spectra associated with the electrochemical cycling has been established and suggests the occurrence of reversible oxidation/reduction processes (redox switching). The four neutral compounds exhibit second-order NLO responses and the β values measured *via* the HLS technique at 1.91 μm in dichloromethane are relatively large for such very simple structures. Oxidation has a dramatic effect on the first hyperpolarisability, causing a doubling of the β value in the case of the mononuclear Ni(II) species and reducing it by half in the case of the heterobimetallic complex [(Fc-ONO)Ni(PyMP)]. The present work validates the use of [(R-ONO)M(PyMP)] units as potential molecular switches, and work aimed at better controlling reversible structural changes is underway.

Experimental

General Considerations

All the reactions were carried out under a dry argon atmosphere using standard Schlenk techniques. The solvents were dried and distilled according to standard procedures.³⁹ The Schiff base ligand precursors An-ONOH₂ and Fc-ONOH₂,¹⁸ and the pyridylmethylenepyran ligand (PyMP)²¹ were synthesized according to literature procedures. All other chemicals were purchased from commercial sources and used without further purification. Solid-state FT-IR spectra were recorded on a Perkin-Elmer, model Spectrum One, FT-IR spectrophotometer with KBr disks in the 4000 to 400 cm⁻¹ range. The ¹H NMR spectra of the diamagnetic complexes **1** and **3** were measured on a Bruker Avance-III 400 Instrument, and are reported in parts per million (ppm, δ) relative to tetramethylsilane (Me₄Si), with the residual solvent proton resonance used as internal standards. Coupling constants (*J*) are reported in Hertz (Hz), and integrations are reported as number of protons. The following abbreviations are used to describe peak patterns: br = broad, s = singlet, d = doublet, t = triplet, m = multiplet. ¹H-NMR chemical shift assignments are given according to the numbering scheme of Chart S1 (ESI[†]). High resolution electro-spray ionization mass spectra (ESI-MS) were acquired on Bruker MAXI 4G and Thermo Fisher Scientific Q-Exactive spectrometers at the Centre Régional de Mesures Physiques de l'Ouest (CRMPO, Université de Rennes 1, France). Elemental analyses were conducted on a Thermo-Finnigan Flash EA 1112 CHNS/O analyzer by the Microanalytical Service of the CRMPO. Melting points were determined in evacuated capillaries on a Kofler Bristoline melting point apparatus and were not corrected.

Synthesis

[[{4-MeO-C₆H₄-C(O)CH=C(CH₃)N-*o*-C₆H₄-2-O}Ni{NC₅H₄-CH=C₅H₂O(Ph)₂}] (1). A Schlenk tube was charged with a magnetic stir bar, 153 mg (0.54 mmol) of An-ONOH₂, 169 mg (1.5 mmol) of potassium *tert*-butoxide and 1.5 mL of THF. After 5 min of stirring, a dark red precipitate was formed and the reaction mixture was vigorously stirred for additional 25 min. Then, a solution of pyridylmethylenepyran (PyMP) (250 mg, 0.77 mmol) in 5 mL of THF was added dropwise. After 10 min of stirring, a solution of Ni(NO₃)₂·6H₂O (145 mg, 0.5 mmol) in 3.5 mL of THF was added dropwise and the stirring was continued overnight. The reaction was quenched with 10 mL of EtOH giving a light brown precipitate. The solid material was filtered off, washed with 4 x 10 mL of cold THF-EtOH mixture (1 : 8), diethyl

ether (3 x 10 mL), and dried under vacuum for 2 h. Single crystals were obtained by slow evaporation of a solution of the compound in dichloromethane (4 days), affording 258 mg (72%) of dark red microcrystals. A crystal from this crop was used for X-ray structure determination. M.p. 170-172 °C. Anal. calcd for C₄₀H₃₂N₂O₄Ni·0.4CH₂Cl₂ (697.4 g mol⁻¹): C, 69.51; H, 4.85; N, 4.01. Found: C, 69.72; H, 4.75; N, 4.21. FT-IR (KBr, cm⁻¹): 3047(w) ν(C–H aryl), 2930(w) ν(C–H alkyl), 2830(w) ν_{sym}(CH₃), 1600(s), 1550(s) ν(C≡O), ν(C≡N) and/or ν(C≡C), 1240(s) ν_{asym}(CH₃-O-aryl), 761(s) δ(C–H). ¹H NMR (400 MHz, CDCl₃): δ_H 2.49 (s, 3 H, CH₃), 3.73 (s, 3 H, OCH₃), 5.22 (s, 1 H, H-9), 5.32 (s, CH₂Cl₂), 5.81 (s, 1H, H-23), 6.37 (t, ³J_{H,H} = 7.4 Hz, 1 H, H-4), 6.64 (d, ³J_{H,H} = 7.3 Hz, 1 H, H-6), 6.75 (br t, ³J_{H,H} = 7.4 Hz, 1 H, H-5), 6.98 (s, 1 H, H-28), 7.18 (s, 1 H, H-25), 7.24 (br m, 5 H, H-3, 12, 16, 19 and 21), 7.40 (m, 2 H, H-32 and 38), 7.50 (d, ³J_{H,H} = 7.8 Hz, 2 H, H-13 and 15), 7.59 (t, ³J_{H,H} = 7.5 Hz, 4 H, H-31, 33, 37 and 39), 7.71 (br s, 4 H, H-30, 34, 36 and 40), 8.44 (br s, 2 H, H-18 and 22).

[[4-MeO-C₆H₄-C(O)CH=C(CH₃)N-C₆H₄-2-O]Cu{NC₅H₄-CH=C₅H₂O(Ph)₂}] (2). This complex was synthesized following a procedure similar to that described above for **1**, using in this case: 153 mg (0.54 mmol) of An-ONOH₂, 169 mg (1.5 mmol) of potassium *tert*-butoxide, 1.5 mL of THF, 250mg (0.77 mmol) of PyMP and a solution of Cu(NO₃)₂·3H₂O (121 mg, 0.54 mmol) in 1.5 mL of THF. Yield: 506 mg (74%) of a light-brown microcrystalline solid. Suitable single crystals for X-ray diffraction analysis were obtained by very slow evaporation of a solution of the compound in dichloromethane (9 days). M.p. 165-170 °C. Anal. calcd for C₄₀H₃₂N₂O₄Cu (668.24 g mol⁻¹): C, 71.89; H, 4.83; N, 4.19. Found: C, 71.51; H, 5.02; N, 4.21. ESI-MS (m/z), calcd for C₄₀H₃₂N₂O₄⁶³Cu: 667.16581, found: 667.1651 (0 ppm) [M⁺]. FT-IR (KBr, cm⁻¹): 3065(w) ν(C–H aryl), 2944(w) ν(C–H alkyl), 2830(w) ν_{sym}(CH₃), 1645(s), 1495(s) ν(C≡O), ν(C≡N) and/or ν(C≡C), 1256(s) ν_{asym}(CH₃-O-aryl), 770(s) δ(C–H).

[[CpFe(η⁵-C₅H₄)–C(O)CH=C(CH₃)N-C₆H₄-2-O]Ni{NC₅H₄-CH=C₅H₂O(Ph)₂}] (3). This complex was synthesized following a procedure similar to that described for complex **1**, using in this case 207 mg (0.57 mmol) of Fc-ONOH₂, 169 mg (1.5 mmol) of potassium *tert*-butoxide, 1.5 mL of THF, 250 mg (0.77 mmol) of PyMP, and a solution of Ni(NO₃)₂·6H₂O (166 mg, 0.57 mmol) in 1.5 mL of THF. Yield: 506 mg (75%) of a brown microcrystalline solid. Single crystals suitable for X-ray diffraction analysis were obtained by slow evaporation of a solution of the compound in dichloromethane (7 days). M.p. 168-170 °C. Anal. calcd for C₄₃H₃₄N₂O₃FeNi (741.28 g mol⁻¹): C, 69.67, H, 4.62 ; N, 3.78. Found: C,

69.34 ; H, 4.68 ; N, 3.70. FT-IR (KBr, cm^{-1}): 3118-3080(w) $\nu(\text{C-H aryl})$, 2926(w) $\nu(\text{C-H alkyl})$, 1606(m), 1562(s) $\nu(\text{C}\equiv\text{O})$, $\nu(\text{C}\equiv\text{N})$ and/or $\nu(\text{C}\equiv\text{C})$, 1504(m)-1408(s) $\nu(\text{C}\equiv\text{C})$ pyridyl, 754(s) $\delta(\text{C-H})$. $^1\text{H NMR}$ (400 MHz, CDCl_3): δ_{H} 2.45 (s, 3 H, CH_3), 4.09 (s, 5 H, Cp), 4.20 (br s, 2 H, $\text{H}_\beta\text{-C}_5\text{H}_4$), 4.45 (br s, 2 H, $\text{H}_\alpha\text{-C}_5\text{H}_4$), 5.50 (s, 1 H, H-9), 5.74 (s, 1 H, H-26), 6.36 (t, $^3J_{\text{H,H}} = 7.5$ Hz, 1 H, H-4), 6.44 (br s, 1 H, H-31), 6.66 (d, $^3J_{\text{H,H}} = 7.7$ Hz, 1 H, H-6), 6.74 (t, $^3J_{\text{H,H}} = 7.5$ Hz, 1 H, H-5), 7.02 (br s, 1 H, H-28), 7.24 (m, 5 H, H-3, 22, 24, 35 and 41), 7.41 (m, 4 H, H-34, 36, 40 and 42), 7.73 (br m, 4 H, H-33, 37, 39 and 43), 8.41 (d, $^3J_{\text{H,H}} = 6.0$ Hz, 2 H, H-21 and 25).

[{CpFe($\eta^5\text{-C}_5\text{H}_4$)-C(O)CH=C(CH₃)N-C₆H₄-2-O}Cu{NC₅H₄-CH=C₅H₂O(Ph)₂}] (4). This complex was synthesized following a procedure similar to that described for complex **1**, using in this case, 207 mg (0.57 mmol) of Fc-ONOH₂, 169 mg (1.5 mmol) of potassium *tert*-butoxide, 1.5 mL of THF, 250 mg (0.77 mmol) of PyMP, and a solution of $\text{Cu}(\text{NO}_3)_2 \cdot 3\text{H}_2\text{O}$ (138 mg, 0.57 mmol) in 1.5 mL of THF. Yield: 506 mg (75%) of a brown microcrystalline solid. Suitable single crystals of **4'** for X-ray diffraction analysis were obtained by very slow evaporation of a solution of compound **4** in dichloromethane (9 days) (see Scheme S2, ESI[†]). M.p. 163-166 °C. Anal. calcd for $\text{C}_{43}\text{H}_{34}\text{N}_2\text{O}_3\text{FeCu}$ (746.13 g mol⁻¹): C, 69.22; H, 4.59; N, 3.75. Found: C, 68.80; H, 4.68; N, 3.76. ESI-MS (*m/z*), calcd for $\text{C}_{43}\text{H}_{34}\text{N}_2\text{O}_3^{63}\text{Cu}^{56}\text{Fe}$: 745.12093, found: 745.120 (1 ppm) [M^+]. FT-IR (KBr, cm^{-1}): 3111-3050(w) $\nu(\text{C-H aryl})$, 1607(w), 1567(s) $\nu(\text{C}\equiv\text{O})$, $\nu(\text{C}\equiv\text{N})$ and/or $\nu(\text{C}\equiv\text{C})$, 1504(m)-1412(s) $\nu(\text{C}\equiv\text{C})$ pyridyl, 753(s) $\delta(\text{C-H})$.

X-ray crystal structure determinations

A crystal of appropriate size and shape of compounds **1**, **2**, **3** and **4'** was coated in Paratone-N oil, mounted on a cryoloop and transferred to the cold gas stream of the cooling device. Intensity data were collected at $T = 150(2)$ K on a Bruker APEXII AXS diffractometer using Mo- $\text{K}\alpha$ radiation ($\lambda = 0.71073$ Å), equipped with a bidimensional CCD detector. The diffraction frames were integrated using the SAINT package,⁴⁰ and corrected by absorption with SABADS.⁴¹ The four structures were solved by dual-space algorithm using the SHELXT program,⁴² and then refined with full-matrix least-square method based on F^2 (SHELXL-2014).⁴³ All non-hydrogen atoms were refined with anisotropic atomic displacement parameters. Hydrogen atoms were placed in their geometrically idealized positions and constrained to ride on their parent atoms. A summary of the details about the data collection

and refinement for the X-ray structures of the four compounds are documented in Table 5, and additional crystallographic details are in the CIF files (ESI[†]). ORTEP views were drawn using OLEX2 program.⁴⁴

Table 5 Crystal data, details of data collection and structure refinement parameters for compounds **1**, **2**, **3** and **4**'.

	1	2	3	4 '
Empirical formula	C ₄₀ H ₃₂ N ₂ NiO ₄	C ₄₀ H ₃₂ CuN ₂ O ₄	C ₄₃ H ₃₄ FeN ₂ NiO ₃	C ₈₆ H ₆₈ Cu ₂ Fe ₂ N ₄ O ₆
Formula weight	663.39	668.21	741.28	1492.22
Collection T (K)	150(2)	150(2)	150(2)	150(2)
Crystal size (mm)	0.32 x 0.23 x 0.09	0.23 x 0.06 x 0.04	0.39 x 0.05 x 0.04	0.20 x 0.14 x 0.04
Color	black	Brown	Red	Brown
Crystal system	Monoclinic	Orthorhombic	Monoclinic	Triclinic
space group	P2 ₁ /n	P2 ₁ cn	P2 ₁ /c	P-1
a (Å)	6.0553(2)	6.3210(3)	21.8315(7)	9.5840(7)
b (Å)	28.0406(9)	17.7556(9)	5.8706(2)	11.8007(9)
c (Å)	18.5892(6)	28.2853(17)	26.5283(9)	15.5930(15)
α (°)	90	90	90	79.465(4)
β (°)	91.3880(10)	90	101.9990(10)	75.558(4)
γ (°)	90	90	90	77.413(5)
V (Å ³)	3155.41(18)	3174.5(3)	3325.69(19)	1651.3(2)
Z	4	4	4	1
D _{calcd} (g.cm ⁻³)	1.396	1.398	1.481	1.501
Abs. coeff. (mm ⁻¹)	0.662	0.734	1.048	1.129
F(000)	1384	1388	1536	770
θ range (°)	3.09 to 27.48	3.10 to 27.48	2.96 to 27.48	3.05 to 27.48
range h, k, l	-5/7, -36/36, -24/24	-8/5, -23/21, -36/35	-28/22, -7/6, -34/34	-12/12, -15/15, -20/20
No. Refl. collected	27756	15906	28226	22734
No. Independent Refl.	7217	5792	7642	7511
Comp. to θ _{max} (%)	99.7	99.8	99.8	99.0
Max/min transmission	0.942/0.856	0.971/0.761	0.959/0.851	0.956/0.814
Data / restraints / parameters	7217/0/426	5792/1/426	7642/0/452	7511/0/452
Final R indices [I>2σ(I)]	R ₁ = 0.0458 wR ₂ = 0.1119	R ₁ = 0.0743 wR ₂ = 0.1070	R ₁ = 0.0405 wR ₂ = 0.0871	R ₁ = 0.0524 wR ₂ = 0.1017
R indices (all data)	R ₁ = 0.0789 wR ₂ = 0.1331	R ₁ = 0.1105 wR ₂ = 0.1190	R ₁ = 0.0802 wR ₂ = 0.1024	R ₁ = 0.0864 wR ₂ = 0.1146
Goodness-of-fit on (F ²)	0.931	1.126	1.004	1.006
Largest diff. peak/hole (e Å ⁻³)	0.475/-0.345	0.470/-0.528	0.402/-0.421	0.446/-0.447

Electrochemical and spectroelectrochemical measurements

Electrochemical studies of all compounds were performed with a home designed three-electrode cell (WE: Pt disk, RE: Ag/AgCl, CE: Tungsten wire). ferrocene (FcH) was added as an internal standard at the end of each experiment to determine redox potential values. The ferrocene/ferrocenium (FcH/FcH⁺) couple was located at $E_{1/2} = 0.42$ V ($\Delta E_p = 96$ mV), where $E_{1/2}$ was calculated from the average of the oxidation and reduction peak potentials. The potential of the cell was controlled by an Autolab PGSTAT 12 driven by the GPES software (Metrohm). Extra-dry dichloromethane (Acros) was used as received. The supporting salt [*n*-Bu₄N][PF₆] was synthesized from NBu₄NOH (Acros) and HPF₆ (Aldrich). It was purified, dried under vacuum for 48h at 100°C, and kept under nitrogen. Thin-layer UV–vis spectroelectrochemistry was performed in a Jacomex glovebox with a specific home-designed cell in a reflectance mode (WE: Pt disk, RE: Pt wire, CE: Pt wire) with an optical path of 0.2 mm. The UV–vis optic fiber probe used was purchased from Ocean Optics. Time-resolved UV–vis detection was performed with a QEPro spectrometer (Ocean optics).

HLS measurements

For the second-order NLO measurements of the Schiff-base chromophores **1-6**, Harmonic Light Scattering (HLS)⁴⁵ was performed using a 10 Hz repetition-rate nanosecond Nd³⁺:YAG laser to obtain the first-order hyperpolarizabilities (β). The measurements at a fundamental wavelength of 1.91 μ m were carried out with 10⁻² M solutions of **1-6** in dichloromethane. The solvent appears to be transparent at 1.91 μ m. A concentrated (10⁻² M) solution of ethyl violet (its octupolar β value being 170 x 10⁻³⁰ esu at 1.91 μ m) was used as external reference.⁴⁶ By using a wavelength of 1.91 μ m, the harmonics at 955 nm remains far from any resonance of the molecules, then preventing from the contribution of possible two-photon fluorescence emission to the HLS signal. We verified the absence of any wide-band two-photon fluorescence by checking that no HLS signal could be detected for wavelengths other than 955 nm. The experimental setup and details of data analysis have been described previously.⁴⁷

Computational details

Geometry optimizations were performed by DFT calculations with the Gaussian 09 package,⁴⁸ using the PBE0 functional⁴⁹ and the all-electron Def2-TZVPP set from EMS Basis Set Exchange Library.⁵⁰ All the optimized geometries were characterized as true minima on their potential energy surface by harmonic vibrational analysis. The UV–visible transitions

were calculated by means of TD-DFT calculations,⁵¹ on the DFT-optimized geometries and at the same PBE0/Def2-TZVP level. Only singlet-singlet transitions were computed.

Conflicts of Interest

The authors declare no conflict of interest.

Acknowledgements

The authors thank P. Hamon (ISCR, Rennes) and P. Jéhan (CRMPO, Rennes) for helpful assistance with NMR and HR-MS measurements, respectively. This research has been performed as part of the Chilean-French International Associated Laboratory for “Multifunctional Molecules and Materials“ (LIA M3-CNRS N°1207). Financial support from the Fondo Nacional de Desarrollo Científico y Tecnológico [FONDECYT (Chile), grant no. 1130105 (D.C. and C.M.)], the Vicerrectoría de Investigación y Estudios Avanzados, Pontificia Universidad Católica de Valparaíso, Chile (D.C. and C.M.), the CNRS and the Université de Rennes 1 are gratefully acknowledged. The GENCI French national computer center is acknowledged for computational resources (Grant a0050807367). N.C. gratefully thanks Dr. N. Le Poul and UMR 6521 (Université de Bretagne Occidentale, Brest), for helpful discussion and their technical support in spectroelectrochemistry. N.N. thanks also the CONICYT (Chile) and BECAS-CHILE for support of a graduate and Joint Supervision Scholarship (PUCV / UR1).

References

- 1 (a) E. Goovaerts, W. Wenseleers, M.H. García and G.H. Cross, in *Handbook of Advanced Electronic and Photonic Materials and Devices*, Ed. H.S. Nalwa, *Nonlinear Optical Materials*, Academic Press, New York, 2001, Vol. 9, p. 127; (b) *Handbook of Optics IV, Fiber Optics & Nonlinear Optics*, 2nd ed., Eds. M. Nass, J. M. Enoch, E. W. V. Stryland and W. L. Wolfe, McGraw-Hill, New York, 2001; (c) *Nonlinear Optical Properties of Mater: From Molecules to Condensed Phases*, Eds. M. G. Papadopoulos, A. J. Sadlej and J. Leszczynski, Springer, India, 2006; (d) *Materials for Nonlinear Optics: Chemical Perspectives*, Eds. S. R. Marder, J. E. Sohn and G. D. Stucky, ACS Symposium Series 455, American Chemical Society, Washington, DC, 1991; (e) P. N. Prasad and D. J. Williams, *Nonlinear Optical Effects In Molecules and Polymers*, Wiley & Sons, New York, 1991; (f) J. Zyss, *Molecular Nonlinear Optics: Materials, Physics and Devices*, Academic Press, Boston, 1994; (g) *Optical Nonlinearities in Chemistry*, Ed. D. M. Burland, *Chem. Rev.*, 1994, **94**, 1; (h) T. Verbiest, S. Houbrechts, M. Kauranen, K. Clays and A. Persoons, *J. Mater. Chem.*, 1997, **7**, 2175-2189; (i) J. A. Delaire and K. Nakatani, *Chem. Rev.*, 2000, **100**, 1817-1845.
- 2 (a) L. T. Cheng, W. Tam, S. H. Stevenson, G. R. Meredith, G. Rikken and S. R. Marder, *J. Phys. Chem.*, 1991, **95**, 10631-10643; (b) L.-T. Cheng, W. Tam, S. R. Marder, A. E. Stirgman, G. Rikken and C. W. Sprangler, *J. Phys. Chem.*, 1991, **95**, 10643-10652.
- 3 (a) *Nonlinear Optical Properties of Organic Molecules and Crystals*, Eds. D. S. Chemla and J. Zyss, Academic Press, Orlando, 1987, Vols. 1 and 2; (b) *Organic Materials for Nonlinear Optics II*, Eds. R. A. Hann and D. Bloor, Royal Society of Chemistry, London, 1991; (c) *Organic Molecules for Nonlinear Optics and Photonics*, Eds. J. Messier, F. Kajzar and P. Prasad, Kluwer Academic Publishers, Dordrecht, The Netherlands, 1991; (d) *Nonlinear Optics of Organic Molecules and Polymers*, Eds. H. S. Nalwa and S. Miyata, CRC Press, New York, 1997; (e) M. G. Kuzyk, M. Eich and R. A. Norwood, *Linear and Nonlinear Optics of Organic Materials III*, Proceedings of SOIE, SPIE, San Diego, 2003, p. 4; (f) N. N. Leclerc, S. Sanaur, L. Galmiche, F. Mathevet, A. J. Attias, J. L. Fave, J. Roussel, P. Hapiot, N. Lemaytre and B. Geffroy, *Chem. Mater.*, 2005, **17**, 502-513.
- 4 For reviews, see for instance: (a) S. Di Bella, C. Dragonetti, M. Pizzotti, D. Roberto, F. Tessore and R. Ugo, in *Topics in Organometallic Chemistry*, Eds. H. Le Bozec and V. Guerschais, *Molecular Organometallic Materials for Optics*, Springer, 2010, vol. 28, p. 1-55; (b) M. G. Humphrey, T. Schwich, P. J. West, M. P. Cifuentes and M. Samoc, in *Comprehensive Inorganic Chemistry II*, Eds. J. Reedijk and K. Poeppelmeier, *Nonlinear Optical Properties of Coordination and Organometallic Complexes*, Elsevier, Oxford, UK, 2013, vol. 8, p. 781-835.
- 5 Selected examples: (a) E. Kulasekera, S. Petrie, R. Stranger and M. G. Humphrey, *Organometallics*, 2014, **33**, 2434-2447. (b) B. J. Coe, S. P. Foxon, R. A. Pilkington, S. Sánchez, D. Whittaker, K. Clays, G. Depotter and B. S. Brunshwig, *Organometallics*, 2015, **34**, 1701-1715; (c) C. Dragonetti, A. Colombo, M. Fontani, D. Marinotto, F. Nisic, S. Righetto, D. Roberto, F. Tintori and S. Fantacci, *Organometallics*, 2016, **35**, 1015-1021; (d) L. E. R. Buckley, B. J. Coe, D. Rusanova, S. Sánchez, M. Jirásek, V. D. Joshi, J. Vávra, D. Khobragade, L. Pospíšil, Š. Ramešová, I. Císařová, D. Šaman, R. Pohl, K. Clays, N. Van Steerteghem, B. S. Brunshwig and F. Teplý, *Dalton Trans.*, 2017, **46**, 1052-1064; (d) R. J. Durand, S. Achelle, S. Gauthier, N. Cabon, M. Ducamp, S. Kahlal, J.-Y. Saillard, A. Barsella and F. Robin-Le Guen, *Dyes Pigm.*, 2018, **155**, 68-74; (e) M. Fontani, E. Garoni, A.

- Colombo, C. Dragonetti, S. Fantacci, H. Doucet, J.-F. Soulé, J. Boixel, V. Guerschais and D. Roberto, *Dalton Trans.*, 2019, **48**, 202-208.
- 6 For reviews, see for instance: (a) P. G. Lacroix, I. Malfant and C. Lepetit, *Coord. Chem. Rev.*, 2016, **308**, 381-394; (b) B. J. Coe, *Coord. Chem. Rev.*, 2013, **257**, 1438-1458; (c) O. Maury and H. Le Bozec, in *Molecular Materials*, Eds. D. W. Bruce, D. O'Hare and R. I. Walton, *Metal-Based Quadratic Nonlinear Optical Materials*, John Wiley & Sons, Ltd, Chichester, UK, 2010, Chapter 1, p. 1-59; (d) B. J. Coe and N. R. M. Curati, *Comments Inorg. Chem.*, 2004, **25**, 147-184; (e) S. Di Bella, *Chem. Soc. Rev.*, 2001, **30**, 355-366.
- 7 Selected examples: (a) L. Rigamonti, F. Demartin, A. Forni, S. Righetto and A. Pasini, *Inorg. Chem.*, 2006, **45**, 10976-10989; (b) I. González, D. Cortés-Arriagada, P. Dreyse, L. Sanhueza-Vega, I. Ledoux-Rak, D. Andrade, I. Brito, A. Toro-Labbé, M. Soto-Arriaza, S. Caramori and B. Loeb, *Eur. J. Inorg. Chem.*; 2015, 4946-4955; (c) T. Guerrero, P. G. Lacroix, H. García-Ortega, O. G. Morales-Saavedra, D. Agustin and N. Farfán, *Inorg. Chim. Acta*, 2016, **442**, 10-15; (d) A. Boulmier, A. Vacher, D. Zang, S. Yang, A. Saad, J. Marrot, O. Oms, P. Mialane, I. Ledoux, L. Ruhlmann, D. Lorcy, and A. Dolbecq, *Inorg. Chem.*, 2018, **57**, 3742-3752; (e) B. Mohan, A. Jana, N. Das, S. Bharti, M. Choudhary, S. Muhammad, S. Kumar, A. G. Al-Sehemi and H. Algarni, *Inorg. Chim. Acta*, 2019, **484**, 148-159.
- 8 (a) M. G. Humphrey, *Aust. J. Chem.*, 2018, **71**, 731-742; (b) V. Guerschais, J. Boixel and H. Le Bozec, In *Photon-Working Switches*, Eds. Y. Yokoyama and K. Nakatani, *Linear and Nonlinear Optical Molecular Switches Based on Photochromic Metal Complexes*, Springer, Tokyo, Japan, 2017, p. 363-384; (c) P. G. Lacroix, I. Malfant, J.-A. Real and V. Rodriguez, *Eur. J. Inorg. Chem.*, 2013, 615-627; (d) K. A. Green, M. P. Cifuentes, M. Samoc and M. G. Humphrey, *Coord. Chem. Rev.*, 2011, **255**, 2530-2541; (e) B. J. Coe, *Acc. Chem. Res.*, 2006, **39**, 383-393; (f) I. Asselberghs, K. Clays, A. Persoons, M. D. Ward and J. McCleverty, *J. Mater. Chem.*, 2004, **14**, 2831-2839.
- 9 (a) X. Liu, C. Ji, Z. Wu, L. Li, S. Han, Y. Wang, Z. Sun and J. Luo, *Chem. Eur. J.*, 2019, **25**, 2610-2615; (b) S. Di Bella, I.P. Oliveri, A. Colombo, C. Dragonetti, S. Righetto and D. Roberto, *Dalton Trans.*, 2012, **41**, 7013-7016; (c) I. Asselberghs, Y. Zhao, K. Clays, A. Persoons, A. Comito and Y. Rubin, *Chem. Phys. Lett.*, 2002, **364**, 279-283.
- 10 T. Guerrero, R. Santillan, H. Garcia-Ortega, O. G. Morales-Saavedra, N. Farfan and P. G. Lacroix, *New J. Chem.*, 2017, **41**, 11881-11890.
- 11 (a) X. Xue, H. Wang, Y. Han and H. Hou, *Dalton Trans.*, 2018, **47**, 13-22; (b) F. Bondu, J. Quertinmont, V. Rodriguez, J.-L. Pozzo, A. Plaquet, B. Champagne and F. Castet, *Chem. Eur. J.*, 2015, **21**, 18749-18757; (c) J. Boixel, V. Guerschais, H. Le Bozec, D. Jacquemin, A. Amar, A. Boucekkine, A. Colombo, C. Dragonetti, D. Marinotto, D. Roberto, S. Righetto and R. De Angelis, *J. Am. Chem. Soc.*, 2014, **136**, 5367-5375; (d) L. Ordronneau, V. Aubert, V. Guerschais, A. Boucekkine, H. Le Bozec, A. Singh, I. Ledoux and D. Jacquemin, *Chem. Eur. J.*, 2013, **19**, 5845-5849.
- 12 Selected examples: (a) M. P. Cifuentes, C. E. Powell, M. G. Humphrey, G. A. Heath, M. Samoc and B. Luther-Davies, *J. Phys. Chem. A*, 2001, **105**, 9625-9627; (b) F. Paul, K. Costuas, I. Ledoux, S. Deveau, J. Zyss, J.-F. Halet and C. Lapinte, *Organometallics*, 2002, **21**, 5229-5235; (c) C.-G. Liu, W. Guan, P. Song, L.-K. Yan and Z.-M. Su, *Inorg. Chem.*, 2009, **48**, 6548-6554; (d) W.-Y. Wang, N.-N. Ma, S.-L. Sun and Y.-Q. Qiu, *Organometallics*, 2014, **33**, 3341-3352.
- 13 B. J. Coe, S. Houbrechts, I. Asselberghs and A. Persoons, *Angew. Chem. Int. Ed.*, 1999, **38**, 366-369.

- 14 M. Malaun, Z. R. Reeves, R. L. Paul, J. C. Jeffery, J. A. McCleverty, M. D. Ward, I. Asselberghs, K. Clays and A. Persoons, *Chem. Commun.*, 2001, 49-50.
- 15 S. Kaur, M. Kaur, P. Kaur, K. Clays and K. Singh, *Coord. Chem. Rev.*, 2017, **343**, 185-219.
- 16 X. Liu, C. Manzur, N. Novoa, S. Celedon, D. Carrillo and J.-R. Hamon, *Coord. Chem. Rev.*, 2018, **357**, 144-172.
- 17 (a) S. Di Bella, A. Colombo, C. Dragonetti, S. Righetto and D. Roberto, *Inorganics*, 2018, **6**, 133; doi:10.3390/inorganics6040133; (b) C. R. Nayar and R. Ravikumar, *J. Coord. Chem.*, 2014, **67**, 1-16; (c) P. G. Lacroix, *Eur. J. Inorg. Chem.*, 2001, 339-348; (d) S. Di Bella and I. Fragalà, *Synth. Met.*, 2000, **115**, 191-196.
- 18 N. Novoa, T. Roisnel, P. Hamon, S. Kahlal, C. Manzur, H. M. Ngo, I. Ledoux-Rak, J.-Y. Saillard, D. Carrillo and J.-R. Hamon, *Dalton Trans.*, 2015, **44**, 18019-18037.
- 19 N. Novoa, T. Roisnel, V. Dorcet, O. Cador, C. Manzur, D. Carrillo and J.-R. Hamon, *New J. Chem.*, 2016, **40**, 5920-5929.
- 20 F. Ba, N. Cabon, F. Robin-Le Guen, P. Le Poul, N. Le Poul, Y. Le Mest, S. Golhen and B. Caro, *Organometallics*, 2008, **27**, 6396-6399.
- 21 F. Ba, F. Robin-Le Guen, N. Cabon, P. Le Poul, S. Golhen, N. Le Poul and B. Caro, *J. Organomet. Chem.*, 2010, **695**, 235-243.
- 22 F. Ba, N. Cabon, P. Le Poul, S. Kahlal, J.-Y. Saillard, N. Le Poul, S. Golhen, B. Caro and F. Robin-Le Guen, *New J. Chem.*, 2013, **37**, 2066-2081.
- 23 N. Novoa, T. Roisnel, V. Dorcet, J.-R. Hamon, D. Carrillo, C. Manzur, F. Robin-Le Guen and N. Cabon, *J. Organomet. Chem.*, 2014, **762**, 19-28.
- 24 L. Wojcik, F. Michaud, S. Gauthier, N. Cabon, P. Le Poul, F. Gloaguen and N. Le Poul, *J. Org. Chem.*, 2017, **82**, 12395-12405.
- 25 P. W. Antoni and M. M. Hansmann, *J. Am. Chem. Soc.*, 2018, **140**, 14823-14835.
- 26 Y. A. Getmanenko, T. G. Allen, H. Kim, J. M. Hales, B. Sandhu, M. S. Fonari, K. Yu. Suponitsky, Y. Zhang, V. N. Khrustalev, J. D. Matichak, T. V. Timofeeva, S. Barlow, S.-H. Chi, J. W. Perry and S. R. Marder, *Adv. Funct. Mater.*, 2018, **28**, 1804073.
- 27 M. Fakis, G. Tsigaridas, I. Polyzos, V. Giannetas, P. Persephonis, I. Spiliopoulos and J. Mikroyannidis, *Chem. Phys. Lett.*, 2001, **342**, 155-161.
- 28 L. Yang, D. R. Powell and R. P. Houser, *Dalton Trans.*, 2007, 955-964.
- 29 N. Novoa, F. Justaud, P. Hamon, T. Roisnel, O. Cador, B. Le Guennic, C. Manzur, D. Carrillo and J.-R. Hamon, *Polyhedron*, 2015, **86**, 81-88.
- 30 A. W. Addison, T. N. Rao, J. Reedijk, J. van Rijn and G. C. Verschoor, *J. Chem. Soc., Dalton Trans.*, 1984, 1349-1356.
- 31 Selected examples: (a) J. P. Grundhoefer, E. E. Hardy, M. M. West, A. B. Curtiss and A. E.V. Gorden, *Inorg. Chim. Acta*, 2019, **484**, 125-132; (b) S. Banerjee, P. Ghorai, P. Brandão, D. Ghosh, S. Bhuiya, D. Chattopadhyay, S. Das and A. Saha, *New J. Chem.*, 2018, **42**, 246-259; (c) T. Thirunavukkarasu, H. A. Sparkes, K. Natarajan and V.G. Gnanasoundari, *Inorg. Chim. Acta*, 2018, **473**, 255-262; (d) A. K. Ghosh, A. Ali, Y. Singh, C. S. Purohit and R. Ghosh, *Inorg. Chim. Acta*, 2018, **474**, 156-163; (e) S. Mondal, M. Chakraborty, A. Mondal, B. Pakhira, A. J. Blake, E. Sinn and S. K. Chattopadhyay, *New J. Chem.*, 2018, **42**, 9588-9597.
- 32 Note: Potential values were calculated vs FcH, assuming a potential of 0.44 V for the FcH/FcH⁺ couple vs Ag/ AgCl.
- 33 M. Orio, O. Jarjayes, H. Kanso, C. Philouze, F. Neese and F. Thomas, *Angew. Chem. Int. Ed.*, 2010, **49**, 4989-4992.
- 34 (a) S. Achelle, S. Kahlal, J.-Y. Saillard, N. Cabon, B. Caro and F. Robin-Le Guen, *Tetrahedron*, 2014, **70**, 2804-2815; (b) P. Solanke, S. Achelle, N. Cabon, O. Pytela, A. Barsella, B. Caro, F. Robin-Le Guen, J. Podlesný, M. Klikar and F. Bures, *Dyes*

- Pigm.*, 2016, **134**, 129-138; (c) A. B. Marco, N. Martínez de Baroja, S. Franco, J. Garín, J. Orduna, B. Villacampa, A. Revuelto and R. Andreu, *Chem. Asian J.*, 2015, **10**, 188-197; (d) A. B. Marco, P. M. Burrezo, L. Mosteo, S. Franco, J. Garin, J. Orduna, B. Diosdado, B. Villacampa, J. T. López Navarrete, J. Casado and R. Andreu, *RSC Adv.*, 2015, **5**, 231-242.
- 35 A. J. Bard and L. R. Faulkner, *Electrochemical methods: fundamentals and applications*, 2nd ed, John Wiley & Sons, Inc., New York, 2001, p. 471-531.
- 36 S. Gauthier, N. Vologdin, S. Achelle, A. Barsella, B. Caro and F. Robin-le Guen, *Tetrahedron*, 2013, **69**, 8392-8399.
- 37 (a) T. Suzuki, H. Tamaoki, J. Nishida, H. Higuchi, T. Iwai, Y. Ishigaki, K. Hanada, R. Katoono, H. Kawai, K. Fujiwara and T. Fukushima, In *Organic Redox Systems: Synthesis, Properties, and Applications*, Ed.T. Nishinaga, *Redox-Mediated Reversible σ -Bond Formation- Cleavage*, Wiley, 2015, p. 13-38; (b) T. Suzuki, E. Ohta, H. Kawai, K. Fujiwara and T. Fukushima, *Synlett*, 2007, 851-853; (c) T. Suzuki, H. Higuchi, T. Tsuji, J. Nishida, Y. Yamashita and T. Miyashi, In *Chemistry of Nanomolecular Systems*, Eds. T. Nakamura, T. Matsumoto, H. Tada and K. Sugiura, *Dynamic Redox Systems: Toward the Realization of Unimolecular Memory*, Springer, Heidelberg, 2003, p. 3-24; (d) H. Kawai, K. Fujiwara and T. Suzuki, *Org. Biomol. Chem.*, 2005, **3**, 3024-3033; (e) J.-I. Nishida, T. Miyagawa and Y. Yamashita, *Org. Lett.*, 2004, **6**, 2523-2526; (f) A. Peters and N. R. Branda, *J. Am. Chem. Soc.*, 2003, **125**, 3404-3405.
- 38 J. L. Oudar and D. S. Chemla, *J. Chem. Phys.*, 1977, **66**, 2664-2668.
- 39 W. L. F. Armarego and C. L. L. Chai, *Purification of Laboratory Chemicals*, 5th ed., Butterworth-Heinemann, Elsevier Inc., Amsterdam, The Netherlands, 2003.
- 40 SAINT-PLUS (Version 6.02), Bruker Analytical X-Ray Systems Inc., Madison, WI, USA, 1999.
- 41 G. M. Sheldrick, *SADABS* (Version 2.05), Bruker Analytical X-Ray Systems Inc., Madison, WI, USA, 1999.
- 42 G. M. Sheldrick, *Acta Crystallogr., Sect. A*, 2015, **71**, 3-8.
- 43 G. M. Sheldrick, *Acta Crystallogr., Sect. C*, 2015, **71**, 3-8.
- 44 O. V. Dolomanov, L. J. Bourhis, R. J. Gildea, J. A. K. Howard and H. Puschmann, *J. Appl. Crystallogr.*, 2009, **42**, 339-341.
- 45 R. W. Terhune, P. D. Maker and C. M. Savage, *Phys. Rev.*, 1965, **14**, 681-684.
- 46 H. Le Bozec, T. Le Bouder, O. Maury, A. Bondon, I. Ledoux, S. Deveau and J. Zyss, *Adv. Mater.*, 2001, **13**, 1677-1681.
- 47 A. Trujillo, M. Fuentealba, D. Carrillo, C. Manzur, I. Ledoux-Rak, J.-R. Hamon and J.-Y. Saillard, *Inorg. Chem.*, 2010, **49**, 2750-2764.
- 48 *Gaussian 09, Revision E.01*, M. J. Frisch, G. W. Trucks, H. B. Schlegel, G. E. Scuseria, M. A. Robb, J. R. Cheeseman, G. Scalmani, V. Barone, B. Mennucci, G. A. Petersson, H. Nakatsuji, M. Caricato, X. Li, H. P. Hratchian, A. F. Izmaylov, J. Bloino, G. Zheng, J. L. Sonnenberg, M. Hada, M. Ehara, K. Toyota, R. Fukuda, J. Hasegawa, M. Ishida, T. Nakajima, Y. Honda, O. Kitao, H. Nakai, T. Vreven, J. A. Jr. Montgomery, J. E. Peralta, F. Ogliaro, M. Bearpark, J. J. Heyd, E. Brothers, K. N. Kudin, V. N. Staroverov, R. Kobayashi, J. Normand, K. Raghavachari, A. Rendell, J. C. Burant, S. S. Iyengar, J. Tomasi, M. Cossi, N. Rega, J. M. Millam, M. Klene, J. E. Knox, J. B. Cross, V. Bakken, C. Adamo, J. Jaramillo, R. Gomperts, R. E. Stratmann, O. Yazyev, A. J. Austin, R. Cammi, C. Pomelli, J. W. Ochterski, R. L. Martin, K. Morokuma, V. G. Zakrzewski, G. A. Voth, P. Salvador, J. J. Dannenberg, S. Dapprich, A. D. Daniels, Ö. Farkas, J. B. Foresman, J. V. Ortiz, J. Cioslowski and D. J. Fox, Gaussian, Inc., Wallingford CT, 2009.

- 49 (a) J. P. Perdew, M. Ernzerhof and K. Burke, *J. Chem. Phys.*, 1996, **105**, 9982–9985;
(b) J. P. Perdew, K. Burke and M. Ernzerhof, *Phys. Rev. Lett.*, 1996, **77**, 3865–3868;
(c) J. P. Perdew, K. Burke and M. Ernzerhof, *Phys. Rev. Lett.*, 1997, **78**, 1396–1396.
- 50 F. Weigend and R. Ahlrichs, *Phys. Chem. Chem. Phys.*, 2005, **7**, 3297–3305.
- 51 K. Burke and E. K. U. Gross, *A guided tour of Time-Dependent Density Functional Theory*, in *Density Functionals: Theory and Applications*, (Lecture Notes in physics), Vol. 500, D. Joubert Ed., Springer, 1998.

Accepted manuscript